Constraints on Axions from Patchy Screening of the Cosmic Microwave Background

Samuel Goldstein[1,*] Fiona McCarthy,[2,3,4] Cristina Mondino,[5] J. Colin Hill,[1]
Junwu Huang,[5] and Matthew C. Johnson[5,6]
[1]Department of Physics, Columbia University, New York, New York 10027, USA
[2]DAMTP, Centre for Mathematical Sciences, Wilberforce Road, Cambridge CB3 0WA, United Kingdom
[3]Kavli Institute for Cosmology Cambridge, Madingley Road, Cambridge, CB3 0HA, United Kingdom
[4]Center for Computational Astrophysics, Flatiron Institute, 162 5th Avenue, New York, New York 10010, USA
[5]Perimeter Institute for Theoretical Physics, 31 Caroline Street North, Waterloo, Ontario N2L 2Y5, Canada
[6]Department of Physics and Astronomy, York University, Toronto, Ontario M3J 1P3, Canada

(Received 18 September 2024; accepted 27 January 2025; published 26 February 2025)

The resonant conversion of cosmic microwave background (CMB) photons into axions within large-scale structure induces an anisotropic spectral distortion in CMB temperature maps. Applying state-of-the-art foreground cleaning techniques to *Planck* CMB observations, we construct maps of axion-induced "patchy screening" of the CMB. We cross-correlate these maps with data from the unWISE galaxy survey and find no evidence of axions. We constrain the axion-photon coupling, $g_{a\gamma\gamma} \lesssim 2 \times 10^{-12}$ GeV^{-1}, at the 95% confidence level for axion masses in the range 10^{-13} eV $\lesssim m_a \lesssim 10^{-12}$ eV. These constraints are competitive with the tightest astrophysical axion limits in this mass range and are inferred from robust population-level statistics, which makes them complementary to existing searches that rely on modeling of individual systems.

DOI: 10.1103/PhysRevLett.134.081001

Introduction—Axions are one of the most compelling extensions to the standard model of particle physics. Originally, the quantum chromodynamics (QCD) axion was proposed as a solution to the strong *CP* problem [1–4]. However, theoretical interest has expanded to more general "axionlike particles," which couple to two photons via the following Lagrangian:

$$\mathcal{L} \supset -\frac{1}{2} m_a^2 a^2 - \frac{1}{4} g_{a\gamma\gamma} F_{\mu\nu} \tilde{F}^{\mu\nu} a, \qquad (1)$$

where a is the axion [5], m_a is the axion mass, $g_{a\gamma\gamma}$ is the axion-photon coupling, $F_{\mu\nu}$ is the electromagnetic field-strength tensor, and $\tilde{F}_{\mu\nu}$ is its dual. Such axions naturally emerge in many beyond standard model scenarios, including string theory, where they can span a wide range of masses [6–9]. Moreover, axions are a well-motivated dark matter candidate [10–13]. Consequently, there are many ongoing and upcoming lab experiments dedicated to searching for axions across a vast range of masses (see reviews [14–16] and references within).

Astrophysical axion searches typically leverage the interaction term in Eq. (1), which induces photon-axion oscillations in the presence of an external magnetic field. Similar to the Mikheyev-Smirnov-Wolfenstein (MSW) effect in neutrino oscillations [17,18], the probability of photon-axion conversion depends on the properties of the medium through which the photon propagates. Notably, resonant (i.e., enhanced) conversion occurs when the axion mass equals the photon's plasma frequency, which is set by

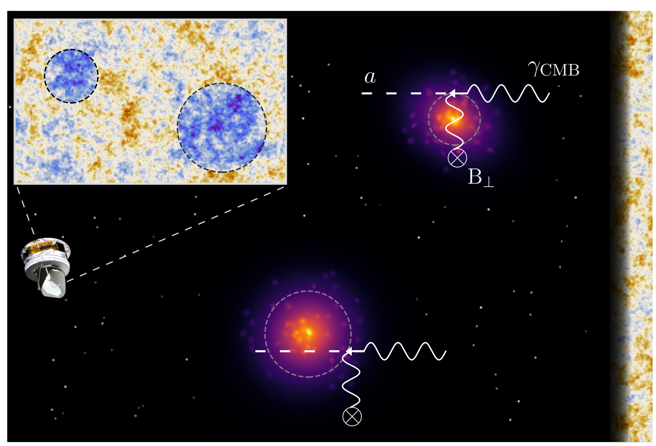

FIG. 1. Illustration of the physical process studied in this Letter: CMB photons ($\gamma_{\rm CMB}$) undergo resonant conversion into axions (a) within the magnetized plasma of galactic halos ($B_\perp$). The dashed circles illustrate the resonance location for the halos, which is set by the free-electron density. The conversion of CMB photons into axions leads to an anisotropic screening of the CMB temperature that is correlated with the positions of galaxies. The inset panel shows the imprint of photon-axion conversion on a CMB temperature map. Note the effect has been greatly amplified for illustrative purposes.

*Contact author: sjg2215@columbia.edu

the free electron density of the medium [19]. Thus, cosmological environments, which typically have low free electron densities and large-scale magnetic fields, provide a powerful setting to search for resonant photon-axion conversions for light-axion models.

The cosmic microwave background (CMB) acts as a natural backlight for exploring photon-axion conversion throughout the Universe. Specifically, the conversion of CMB photons into axions introduces secondary anisotropies in both the intensity and polarization of the CMB [20–27]. In this Letter, we study the resonant conversion of CMB photons into axions as they traverse the ionized gas and magnetic fields within galactic halos. This conversion leads to anisotropic, i.e., "patchy," screening of the CMB temperature that is spatially correlated with the locations of galaxies [21,22,25] (see Fig. 1 for an illustration).

Recently, Ref. [25] derived theoretical predictions for the imprints of axion-induced screening by large-scale structure (LSS) in the CMB and forecasted that an analysis combining *current* galaxy survey and CMB temperature data can provide competitive sensitivity to the axion-photon coupling for $m_a \approx 10^{-13}$ eV axions. In this Letter, we perform the first such analysis. Specifically, we present the first measurement of the cross-correlation between axion-induced CMB screening and the galaxy number density field. We find no evidence for axion-induced screening of the CMB, and constrain the axion-photon coupling $g_{a\gamma\gamma} \lesssim 2 \times 10^{-12}$ GeV^{-1} for axions with mass 10^{-13} eV $\lesssim m_a \lesssim 10^{-12}$ eV. The Supplemental Material (SM) [28] contains further information validating our measurement and theoretical modeling.

Conventions: We work in natural units, $\hbar = k_B = c = 1$. We assume a flat ΛCDM fiducial cosmology based on the *Planck* 2018 analysis [52]: $\Omega_{\rm cdm}h^2 = 0.1201$, $\Omega_{\rm b}h^2 = 0.0224$, $h = 0.6732$, $\ln(10^{10}A_s) = 3.0448$, $n_s = 0.9661$, and $\tau = 0.0543$. Here, $\Omega_{\rm cdm}h^2$ and $\Omega_{\rm b}h^2$ are the present-day physical cold dark matter and baryon densities, respectively, $h \equiv H_0/100$ km/s/Mpc is the dimensionless Hubble constant, A_s and n_s are the amplitude and spectral index of primordial scalar perturbations, respectively, and τ is the optical depth to reionization.

Axion screening of the CMB—We first review the theoretical formalism describing axion-induced screening of the CMB, and its cross-correlation with the galaxy distribution. For more details, see Ref. [25] and the SM of this Letter.

Consider a CMB photon with frequency ν propagating through a halo with free electron density $n_e(\mathbf{x})$ and magnetic field $\mathbf{B}(\mathbf{x})$. The interaction in Eq. (1) leads to a mixing between the component of the photon polarized along the direction of the transverse magnetic field and an ultrarelativistic axion with mass $m_a \ll \nu$. The mixing is most efficient if the axion mass is equal to the in-medium plasma mass, $m_\gamma(\mathbf{x}) \equiv \sqrt{4\pi\alpha n_e(\mathbf{x})/m_e} \approx 3.7 \times 10^{-11}\ \mathrm{eV}\sqrt{n_e/\mathrm{cm}^{-3}}$, where α is the fine-structure constant [53]. In the Landau-Zener approximation, the probability for the photon to resonantly convert into an axion is [19,54,55]

$$P^{\rm res}_{\gamma\to a}[\mathbf{x}(t_{\rm res}), \nu] \simeq \frac{2\pi^2 \nu g^2_{a\gamma\gamma}|\mathbf{B}^{\rm res}_\perp|^2}{m_a^2}\left|\frac{d\ln m_\gamma^2(\mathbf{x})}{dt}\right|^{-1}_{t_{\rm res}}, \quad (2)$$

where $\mathbf{B}^{\rm res}_\perp$ is the component of the magnetic field transverse to the propagation direction of the photon evaluated at the resonance location and $t_{\rm res}$ is the time of resonance.

Equation (2) leads to a spatially anisotropic screening of the CMB temperature which is conveniently described by the dark-screening optical depth [25,56,57],

$$\tau^a(\hat{\boldsymbol{n}}, \nu) = \sum_{t_{\rm res}} P^{\rm res}_{\gamma\to a}[\mathbf{x}(t_{\rm res}), \nu], \quad (3)$$

where the sum is taken over all resonances along the line of sight, $\hat{\boldsymbol{n}}$. Consequently, photon-axion conversion induces an anisotropic spectral distortion in the CMB temperature [58] $\tilde{T}^a(\nu, \hat{\boldsymbol{n}}) = T_{\rm CMB}\tau^a(\nu, \hat{\boldsymbol{n}})[(1 - e^{-x})/x]$, where $x \equiv 2\pi\nu/T_{\rm CMB}$ is the dimensionless frequency, $T_{\rm CMB} \approx 2.726$ K is the CMB monopole temperature, and the term in parentheses accounts for the conversion from specific intensity to CMB thermodynamic temperature units. For convenience, we define the axion screening map at a reference frequency of $\nu = 353$ GHz and label the map as $\tilde{T}^a_{353\ \mathrm{GHz}}(\hat{\boldsymbol{n}})$ when the normalization is relevant.

In this Letter, we investigate the cross-correlation between the axion-induced screened CMB temperature, $\tilde{T}^a(\hat{\boldsymbol{n}})$, and the projected galaxy overdensity, $\delta_g(\hat{\boldsymbol{n}})$. Since both $\tilde{T}^a$ and δ_g are defined on the sphere, it is convenient to work in the spherical harmonic basis. The cross-correlation is then described by the angular cross-power spectrum, $\langle \delta_{g,\ell m}\tilde{T}^a_{\ell' m'}\rangle = \delta^{\rm K}_{\ell\ell'}\delta^{\rm K}_{mm'}C^{g\tilde{T}^a}_\ell$, where $\delta^{\rm K}$ is the Kronecker delta, and we have assumed that $\tilde{T}^a$ and δ_g are statistically isotropic. Not only is $C^{g\tilde{T}^a}_\ell$ more sensitive to $g_{a\gamma\gamma}$ than $C^{\tilde{T}^a\tilde{T}^a}_\ell$ (see Ref. [25] and the SM), but the cross-correlation is immune to biases from foreground contaminants in the axion screening map that are uncorrelated with the galaxy overdensity map.

We model $C^{g\tilde{T}^a}_\ell$ using the halo model formalism in Ref. [25]. We model the galaxy distribution using the halo occupation distribution (HOD) from Ref. [59]. We model the electron distribution using the "active galactic nuclei (AGN) feedback" model from [60]. We model the halo magnetic field using the IllustrisTNG simulations [61]. The IllustrisTNG simulations are state-of-the-art cosmological magnetohydrodynamical simulations that have been shown to reproduce a wide range of observed galaxy properties [62–66]. In this Letter, we compute the spherically averaged, mass-weighted mean magnetic field profiles for halos in the TNG100-1 and TNG300-1 simulations—the highest-resolution runs of the IllustrisTNG $(110.7\ \mathrm{Mpc})^3$ and $(302.6\ \mathrm{Mpc})^3$ comoving-volume simulations, respectively.

We compute the profiles for $10^{11}M_\odot - 10^{15}M_\odot$ halos between redshifts $0 \le z \le 1.5$, covering the range of halo masses and redshifts in our galaxy sample. Because of the limited number of massive halos in the TNG100-1 simulation, we use the TNG300-1 simulation to estimate the magnetic field profiles for halos with $M_{\rm halo} \gtrsim 10^{14} M_\odot$. Our improved magnetic field modeling in massive halos leads to a final constraint that is better than the forecast from Ref. [25]. Finally, we conservatively neglect conversions that occur deep within the halo or in its outermost regions, where theoretical modeling, particularly of the electron distribution and magnetic field, has more uncertainties. Specifically, we only consider conversions that occur between $0.1\ R_{200c} < r < \min(R_{\rm vir}, 1.08\ R_{200c})$, where r is the distance to the halo center, R_{200c} is the radius at which the average density enclosed within the halo equals 200 times the critical density of the Universe at the halo redshift, and $R_{\rm vir}$ is the virial radius. The second upper bound comes from the truncation scale used in the best-fit HOD model for the galaxy sample considered here [59]. In SM, we provide constraints for various models of the electron distribution, magnetic field, and galaxy distribution, and offer additional details regarding the halo model calculation.

Axion screening and galaxy data—From Eq. (3), the resonant conversion of CMB photons into axions causes a spectral distortion in the CMB temperature with the following spectral energy distribution (SED) [67]:

$$\frac{\tilde{T}^a(x)}{T_{\rm CMB}} \propto x\left(\frac{1-e^{-x}}{x}\right), \tag{4}$$

where $x \equiv 2\pi\nu/T_{\rm CMB}$. Consequently, we can leverage the constrained needlet internal linear combination (NILC) method [68–70] to construct maps of axion-induced screening from multifrequency CMB temperature data. In general, the ILC procedure [71–74] constructs the minimum-variance linear combination of the observed frequency maps that ensures unit response to the signal of interest. In NILC, the weights are computed on a frame of needlets [75], which have compact support in both real and harmonic space. NILC is particularly well-suited for CMB analyses since Galactic contributions are often localized in real space, whereas extragalactic contributions are often better described in harmonic space. We use *constrained* NILC [69,76], which exactly removes contributions from unwanted signals in the map that have a known SED, albeit at the cost of increasing the noise of the map. We construct our NILC maps using PYILC [70,77].

For our fiducial analysis, we use the *Planck* NPIPE (PR4) [78] CMB temperature maps at 30, 44, 70, 100, 143, 217, 353, and 545 GHz. Following similar analyses in Refs. [57,70,79], we preprocess the maps by masking the Galactic plane and bright point sources, and subsequently inpainting these masked regions. Since we are interested in cross-correlating our axion map with LSS tracers, we need to use the constrained NILC to "deproject" foreground contaminants that are correlated with the unWISE galaxies, particularly the thermal Sunyaev-Zel'dovich (tSZ) effect [80,81] and the cosmic infrared background (CIB) [82]. The tSZ effect has a known spectral response and can be deprojected exactly. Since there is no exact model for the CIB SED, we follow Refs. [57,70,79] and model the CIB as a modified blackbody. We fix the CIB temperature $T_{\rm CIB} = 20$ K and spectral index $\beta_{\rm CIB} = 1.6$. To account for deviations in the CIB SED from a modified blackbody, we also deproject the first derivative of the SED with respect to $\beta_{\rm CIB}$, following Ref. [85]. The SM presents extensive validation of our map-making and foreground-cleaning procedure.

For our galaxy sample, we use infrared-selected galaxies from the unWISE catalog [86–90] constructed from data collected by the Wide-field Infrared Survey Explorer (WISE) mission [91,92]. The unWISE catalog includes over 500 million galaxies across the full sky, making it particularly well-suited for cross-correlation analyses. In this Letter, we use the low-redshift unWISE "Blue" sample [90], which has a mean redshift of $\bar{z} \approx 0.6$. The unWISE catalog also contains higher-redshift "Green" ($\bar{z} \approx 1.1$) and "Red" ($\bar{z} \approx 1.5$) samples. However, these samples are more strongly correlated with the CIB, which is predominantly sourced by higher-redshift dusty star-forming galaxies [93,94]. Indeed, in the SM we demonstrate that our fiducial analysis methods are insufficient for removing high-redshift CIB contributions that are correlated with the unWISE Green sample, despite their robust performance for the Blue sample. Finally, even in the absence of CIB contamination, modeling the cross-correlation $C_\ell^{g\tilde{T}^a}$ for these high-redshift galaxy samples is challenging due to increased uncertainty in the magnetic field and electron number density models.

Cross-correlation measurement—We compute the angular cross-power spectrum between the axion screening map and the unWISE Blue galaxy catalog using NAMASTER [95–97], which accounts for the mask-induced mode coupling. We mask the galaxy map using the union of the unWISE mask [90] and the Planck CMB lensing mask, leaving 51% of the sky unmasked. We mask the axion map using the union of the preprocessing mask with the Planck 70% Galactic plane mask, leaving 62.5% of the sky unmasked. We estimate the cross-power spectra in multipole bins between $5 < \ell < 3000$ with width $\Delta\ell = 150$. To estimate the covariance of $C_\ell^{g\tilde{T}^a_{353\,\rm GHz}}$, we compute the Gaussian covariance using the improved narrow kernel approximation [98]. Our analysis includes only multipoles with bin centers between $300 \le \ell \le 2000$. As described in SM, we exclude the two bins below $\ell = 300$ to avoid contributions from the ISW effect and to mitigate the impact of possible large-scale residual extragalactic foregrounds present in our axion screening maps. We exclude

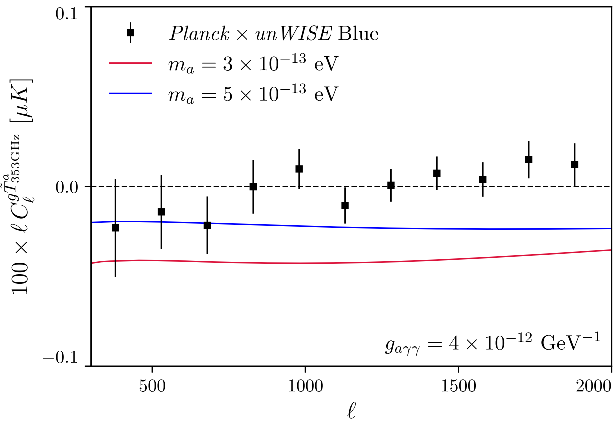

FIG. 2. Measured cross-correlation between our axion screening map and the unWISE Blue galaxy sample. The measurement is consistent with zero (PTE of 0.61), thus we find no evidence of axion-induced screening. The solid lines show halo model predictions for the cross-correlation for two axion masses, assuming $g_{a\gamma\gamma} = 4 \times 10^{-12}$ GeV^{-1}.

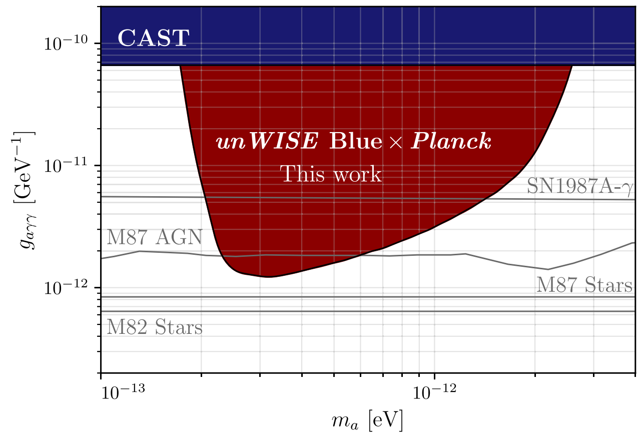

FIG. 3. Constraints on the axion-photon coupling, $g_{a\gamma\gamma}$. The red region indicates the 95% upper exclusion limit on $g_{a\gamma\gamma}$ derived in this Letter. The shaded blue region denotes the 95% bound set by CAST [99]. The solid gray lines show the 95% confidence limits derived from various high-energy astrophysics searches for photon-axion or axion-photon conversion in a *single* galaxy [110], including the absence of spectral distortions in the AGN spectrum of M87 [103], the nonobservation of γ-rays from axions produced in SN1987A and converting within the Galactic magnetic field [100], and the absence of x-ray signals from stellar axion production and conversion in M82 and M87 [104]. We present a more detailed comparison with existing constraints in the text.

bins with $\ell > 2000$ to account for potential limitations in the HOD modeling on smaller scales. Detailed discussions of the cross-power spectrum measurement are provided in SM.

Figure 2 presents the measured cross-power spectrum between our axion-induced screening map and the unWISE Blue galaxy sample, $C_\ell^{g\tilde{T}^a_{353\ \mathrm{GHz}}}$. The measured cross-correlation is consistent with zero, with a χ^2 value of 9.2 for 11 degrees of freedom. This corresponds to a probability to exceed (PTE) of 0.61. Thus, we do not detect axion-induced screening. For comparison, the solid lines in Fig. 2 show the halo model predictions for two different axion masses assuming an axion-photon coupling $g_{a\gamma\gamma} = 4 \times 10^{-12}$ GeV^{-1}. The theoretical prediction for the cross-correlation is negative since photon-axion conversion *decreases* the CMB intensity near galaxies.

Constraints on the axion-photon coupling—Using the measurement and theoretical predictions for $C_\ell^{g\tilde{T}^a_{353\ \mathrm{GHz}}}$, we can exclude regions of the $m_a - g_{a\gamma\gamma}$ plane. We assume a Gaussian likelihood, which is given by, up to a constant,

$$\ln \mathcal{L}(\hat{C}_\ell^{g\tilde{T}^a}|\boldsymbol{\theta}) = \left(\delta C_\ell^{g\tilde{T}^a}(\boldsymbol{\theta})\right)^T \mathcal{C}_{\ell\ell'}^{-1}\left(\delta C_{\ell'}^{g\tilde{T}^a}(\boldsymbol{\theta})\right), \quad (5)$$

where $\boldsymbol{\theta} = (g_{a\gamma\gamma}, m_a)$ is the parameter vector, $\delta C_\ell^{g\tilde{T}^a}(\boldsymbol{\theta})$ is the difference between the measured cross-power spectrum and our theoretical model, and $\mathcal{C}_{\ell\ell'}^{-1}$ is the inverse of the $\hat{C}_\ell^{g\tilde{T}^a}$ covariance matrix, which accounts for the noise and mask-induced mode coupling in our maps. To obtain the posterior distribution of $\boldsymbol{\theta}$, we vary the axion mass over 55 values logarithmically spaced between 10^{-13} eV and 4×10^{-12} eV. For each value of m_a, we sample from the posterior distribution of $g_{a\gamma\gamma}$ assuming a uniform prior on the axion-photon coupling, with $g_{a\gamma\gamma} \geq 0$ GeV^{-1}.

Figure 3 shows the constraints on the axion-photon coupling, $g_{a\gamma\gamma}$, derived in this Letter. The shaded red region shows the 95% one-tailed upper confidence limit on $g_{a\gamma\gamma}$ derived from $C_\ell^{g\tilde{T}^a}$. The shaded blue region shows the laboratory constraints from the CERN Axion Solar Telescope (CAST) [99]. The grey lines depict some of the most stringent astrophysical bounds in this region of parameter space, which are derived from Solar Maximum Mission γ-ray observations of SN1987A [100,101], Chandra x-ray observations of active galactic nuclei (AGN) in M87 [103], and NuSTAR x-ray observations of M82 and M87 [104]. There are also tight bounds on the axion-photon coupling in this mass range from observations of the AGN spectra of NGC 1275 [105] and H1821 + 643 [106]. We do not include these in Fig. 3 for visual clarity, as they overlap with the M82 stellar axion production constraint. We also note that constraints on axions in this mass range that are independent of the axion-photon coupling can be derived from black hole superradiance [107,108]. However, such constraints only apply if the axion self-interaction is small [109].

Conclusions—In this Letter, we have derived new limits on the axion-photon coupling for light axions by analyzing the cross-correlation of galaxies with foreground-cleaned maps of resonant axion-induced screening in the CMB. Utilizing state-of-the-art CMB and LSS datasets, we have constrained the axion-photon coupling

$g_{a\gamma\gamma} \lesssim 2 \times 10^{-12}$ GeV^{-1} at the 95% confidence level for 10^{-13} eV $\lesssim m_a \lesssim 10^{-12}$ eV.

Our constraints are significantly tighter than the laboratory bounds from CAST and are competitive with the most stringent limits from previous astrophysical axion searches. Notably, unlike conventional astrophysical axion searches, which are typically based on photon-axion conversion within a single galaxy, our constraints are derived by searching for *statistically averaged* photon-axion conversion in the circumgalactic medium (CGM) of tens of millions of galaxies. By focusing on photon-axion conversions outside of the halo center, our constraints are less sensitive to the complex modeling of the magnetic field within galaxies. Finally, the photon source in our analysis is the CMB, which has remarkably well-understood statistical and physical properties. Consequently, our constraints are highly complementary to existing astrophysical axion bounds.

There are several possible extensions to this Letter. First, near-term CMB and LSS surveys are expected to improve our constraints by an order of magnitude [25]. Cross-correlating with a higher-redshift tracer could also improve our sensitivity to $m_a \gtrsim 10^{-12}$ eV axions [25]. Additionally, axion-photon conversion produces unique signatures in the CMB polarization that one could search for using similar methods to the analysis in this Letter. On the modeling side, as with all astrophysical axion searches, our constraints depend on assumptions about the electron distribution and magnetic field strength in astrophysical environments. While we have employed state-of-the-art models for the electron density and magnetic field strength within halos, these quantities, particularly the latter, remain subject to considerable uncertainty. Fortunately, significant improvements in understanding these quantities are expected in the near future. For example, measurements of the kinematic Sunyaev-Zel'dovich effect [111–113] and fast radio bursts [114,115] will help model the electron distribution. Furthermore, future observations will better constrain the magnetic field profile around halos [116–118]. These observational improvements will be supported by advancements in cosmological magnetohydrodynamical simulations [119]. In conclusion, the axion search conducted in this Letter not only provides some of the most stringent constraints on 10^{-13} eV $\lesssim m_a \lesssim 10^{-12}$ eV mass axions, but also lays the foundation for future astrophysical searches for these elusive particles using CMB and LSS datasets.

Acknowledgments—We thank Aleksandra Kusiak and Dalila Pîrvu for useful discussions. The authors acknowledge the Texas Advanced Computing Center (TACC) [120] at the University of Texas at Austin for providing computational resources that have contributed to the research results reported within this Letter. We acknowledge computing resources from Columbia University's Shared Research Computing Facility project, which is supported by NIH Research Facility Improvement Grant No. 1G20RR030893-01, and associated funds from the New York State Empire State Development, Division of Science Technology and Innovation (NYSTAR) Contract No. C090171, both awarded April 15, 2010. S. G. and J. C. H. acknowledge support from NSF Grant No. AST-2307727 and DOE HEP Grant No. DE-SC0011941. J. C. H. also acknowledges support from NSF Grant No. AST-2108536, NASA Grants No. 80NSSC22K0721 (ATP) and No. 80NSSC23K0463 (ADAP), the Sloan Foundation, and the Simons Foundation. M. C. J. and J. H. are supported by the Natural Sciences and Engineering Research Council of Canada through a Discovery grant. Research at Perimeter Institute is supported in part by the Government of Canada through the Department of Innovation, Science and Economic Development Canada and by the Province of Ontario through the Ministry of Research, Innovation and Science. F. McC. acknowledges support from the European Research Council (ERC) under the European Union's Horizon 2020 research and innovation programme (Grant Agreement No. 851274). The Flatiron Institute is a division of the Simons Foundation.

[1] R. D. Peccei and H. R. Quinn, Phys. Rev. D **16**, 1791 (1977).
[2] R. D. Peccei and H. R. Quinn, Phys. Rev. Lett. **38**, 1440 (1977).
[3] S. Weinberg, Phys. Rev. Lett. **40**, 223 (1978).
[4] F. Wilczek, Phys. Rev. Lett. **40**, 279 (1978).
[5] Henceforth, we use the term "axion" to refer to any pseudoscalar field coupled to the electromagnetic sector via Eq. (1).
[6] E. Witten, Phys. Lett. B **149**, 351 (1984).
[7] P. Svrcek and E. Witten, J. High Energy Phys. 06 (2006) 051.
[8] A. Arvanitaki, S. Dimopoulos, S. Dubovsky, N. Kaloper, and J. March-Russell, Phys. Rev. D **81**, 123530 (2010).
[9] D. J. E. Marsh, in *Proceedings of the 13th Patras Workshop on Axions, WIMPs and WISPs* (2018), pp. 59–74; arXiv:1712.03018.
[10] J. Preskill, M. B. Wise, and F. Wilczek, Phys. Lett. **120B**, 127 (1983).
[11] L. F. Abbott and P. Sikivie, Phys. Lett. **120B**, 133 (1983).
[12] M. Dine and W. Fischler, Phys. Lett. **120B**, 137 (1983).
[13] L. Hui, Annu. Rev. Astron. Astrophys. **59**, 247 (2021).
[14] P. W. Graham, I. G. Irastorza, S. K. Lamoreaux, A. Lindner, and K. A. van Bibber, Annu. Rev. Nucl. Part. Sci. **65**, 485 (2015).
[15] I. G. Irastorza and J. Redondo, Prog. Part. Nucl. Phys. **102**, 89 (2018).
[16] K. Choi, S. H. Im, and C. Sub Shin, Annu. Rev. Nucl. Part. Sci. **71**, 225 (2021).
[17] L. Wolfenstein, Phys. Rev. D **17**, 2369 (1978).

[18] S. P. Mikheyev and A. Y. Smirnov, Sov. J. Nucl. Phys. **42**, 1441 (1985), https://ui.adsabs.harvard.edu/abs/1985YaFiz.42.1441M.
[19] A. Mirizzi, J. Redondo, and G. Sigl, J. Cosmol. Astropart. Phys. 08 (2009) 001.
[20] M. Schlederer and G. Sigl, J. Cosmol. Astropart. Phys. 01 (2016) 038.
[21] G. D'Amico and N. Kaloper, Phys. Rev. D **91**, 085015 (2015).
[22] S. Mukherjee, R. Khatri, and B. D. Wandelt, J. Cosmol. Astropart. Phys. 04 (2018) 045.
[23] S. Mukherjee, R. Khatri, and B. D. Wandelt, J. Cosmol. Astropart. Phys. 06 (2019) 031.
[24] S. Mukherjee, D. N. Spergel, R. Khatri, and B. D. Wandelt, J. Cosmol. Astropart. Phys. 02 (2020) 032.
[25] C. Mondino, D. Pîrvu, J. Huang, and M. C. Johnson, J. Cosmol. Astropart. Phys. 10 (2024) 107.
[26] H. Mehta and S. Mukherjee, J. Cosmol. Astropart. Phys. 07 (2024) 084.
[27] H. Mehta and S. Mukherjee, J. Cosmol. Astropart. Phys. 09 (2024) 037.
[28] See Supplemental Material at http://link.aps.org/supplemental/10.1103/PhysRevLett.134.081001, which includes Refs. [29–51] for additional details.
[29] M. J. Rees and D. W. Sciama, Nature (London) **217**, 511 (1968).
[30] S. Ferraro, E. Schaan, and E. Pierpaoli, arXiv:2205.10332.
[31] O. Dore, J. F. Hennawi, and D. N. Spergel, Astrophys. J. **606**, 46 (2004).
[32] P. A. R. Ade *et al.* (Planck Collaboration), Astron. Astrophys. **594**, A4 (2016).
[33] R. Adam *et al.* (Planck Collaboration), Astron. Astrophys. **594**, A7 (2016).
[34] A. Kusiak, K. M. Surrao, and J. C. Hill, Phys. Rev. D **108**, 123501 (2023).
[35] J. A. Peacock and R. E. Smith, Mon. Not. R. Astron. Soc. **318**, 1144 (2000).
[36] Z. Zheng, A. L. Coil, and I. Zehavi, Astrophys. J. **667**, 760 (2007).
[37] B. Bolliet, J. C. Hill, S. Ferraro, A. Kusiak, and A. Krolewski, J. Cosmol. Astropart. Phys. 03 (2023) 039.
[38] J. F. Navarro, C. S. Frenk, and S. D. M. White, Astrophys. J. **490**, 493 (1997).
[39] J. L. Tinker, A. V. Kravtsov, A. Klypin, K. Abazajian, M. S. Warren, G. Yepes, S. Gottlober, and D. E. Holz, Astrophys. J. **688**, 709 (2008).
[40] D. N. Limber, Astrophys. J. **119**, 655 (1954).
[41] R. Scoccimarro, R. K. Sheth, L. Hui, and B. Jain, Astrophys. J. **546**, 20 (2001).
[42] A. R. Duffy, J. Schaye, S. T. Kay, and C. Dalla Vecchia, Mon. Not. R. Astron. Soc. **390**, L64 (2008); **415**, L85(E) (2011).
[43] S. Bhattacharya, S. Habib, K. Heitmann, and A. Vikhlinin, Astrophys. J. **766**, 32 (2013).
[44] J. L. Tinker, B. E. Robertson, A. V. Kravtsov, A. Klypin, M. S. Warren, G. Yepes, and S. Gottlober, Astrophys. J. **724**, 878 (2010).
[45] A. Lewis, A. Challinor, and A. Lasenby, Astrophys. J. **538**, 473 (2000).
[46] W. R. Coulton *et al.* (ACT Collaboration), arXiv:2401.13033.
[47] M. C. D. Marsh, J. H. Matthews, C. Reynolds, and P. Carenza, Phys. Rev. D **105**, 016013 (2022), 2107.08040.
[48] D. Nelson, A. Pillepich, M. Ayromlou, W. Lee, K. Lehle, E. Rohr, and N. Truong, arXiv:2311.06338.
[49] B. K. K. Lee, W. R. Coulton, L. Thiele, and S. Ho, Mon. Not. R. Astron. Soc. **517**, 420 (2022).
[50] R. Pakmor, F. van de Voort, R. Bieri, F. A. Gómez, R. J. J. Grand, T. Guillet, F. Marinacci, C. Pfrommer, C. M. Simpson, and V. Springel, Mon. Not. R. Astron. Soc. **498**, 3125 (2020).
[51] N. Battaglia, J. R. Bond, C. Pfrommer, and J. L. Sievers, Astrophys. J. **758**, 75 (2012).
[52] N. Aghanim *et al.* (Planck Collaboration), Astron. Astrophys. **641**, A6 (2020); **652**, C4(E) (2021).
[53] For the halo masses considered here, the electron number density typically varies between 10^{-5} cm$^{-3} \lesssim n_e \lesssim 10^{-3}$ cm^{-3}, hence we are sensitive to axion masses between 10^{-13} eV and 10^{-12} eV.
[54] S. J. Parke, Phys. Rev. Lett. **57**, 1275 (1986).
[55] H. Tashiro, J. Silk, and D. J. E. Marsh, Phys. Rev. D **88**, 125024 (2013).
[56] D. Pîrvu, J. Huang, and M. C. Johnson, J. Cosmol. Astropart. Phys. 10 (2024) 019.
[57] F. McCarthy, D. Pirvu, J. C. Hill, J. Huang, M. C. Johnson, and K. K. Rogers, Phys. Rev. Lett. **133**, 141003 (2024).
[58] We use the notation $\tilde{T}^a$ to denote the temperature fluctuation induced by photon-axion conversion. As described in [22,24–27], photon-axion conversion also introduces polarized spectral distortions. However, this work focuses solely on the CMB temperature distortion, which is projected to provide the best sensitivity for current data.
[59] A. Kusiak, B. Bolliet, A. Krolewski, and J. C. Hill, Phys. Rev. D **106**, 123517 (2022).
[60] N. Battaglia, J. Cosmol. Astropart. Phys. 08 (2016) 058.
[61] D. Nelson *et al.*, Comput. Astrophys. Cosmol. **6**, 2 (2019).
[62] A. Pillepich *et al.*, Mon. Not. R. Astron. Soc. **475**, 648 (2018).
[63] V. Springel *et al.*, Mon. Not. R. Astron. Soc. **475**, 676 (2018).
[64] D. Nelson *et al.*, Mon. Not. R. Astron. Soc. **475**, 624 (2018).
[65] J. P. Naiman, A. Pillepich, V. Springel, E. Ramirez-Ruiz, P. Torrey, M. Vogelsberger, R. Pakmor, D. Nelson, F. Marinacci, L. Hernquist, R. Weinberger, and S. Genel, Mon. Not. R. Astron. Soc. **477**, 1206 (2018).
[66] F. Marinacci *et al.*, Mon. Not. R. Astron. Soc. **480**, 5113 (2018).
[67] We normalize the SED to unity at 353 GHz.
[68] J. Delabrouille, J. F. Cardoso, M. L. Jeune, M. Betoule, G. Fay, and F. Guilloux, Astron. Astrophys. **493**, 835 (2009).
[69] M. Remazeilles, J. Delabrouille, and J.-F. Cardoso, Mon. Not. R. Astron. Soc. **410**, 2481 (2011).
[70] F. McCarthy and J. C. Hill, Phys. Rev. D **109**, 023528 (2024).
[71] C. L. Bennett, G. F. Smoot, G. Hinshaw, E. L. Wright, A. Kogut, G. de Amici, S. S. Meyer, R. Weiss,

D. T. Wilkinson, S. Gulkis, M. Janssen, N. W. Boggess, E. S. Cheng, M. G. Hauser, T. Kelsall, J. C. Mather, J. Moseley, S. H., T. L. Murdock, and R. F. Silverberg, Astrophys. J. Lett. **396**, L7 (1992).
[72] C. Bennett *et al.* (WMAP Collaboration), Astrophys. J. Suppl. Ser. **148**, 97 (2003).
[73] M. Tegmark, A. de Oliveira-Costa, and A. Hamilton, Phys. Rev. D **68**, 123523 (2003).
[74] H. K. Eriksen, A. J. Banday, K. M. Gorski, and P. B. Lilje, Astrophys. J. **612**, 633 (2004).
[75] F. J. Narcowich, P. Petrushev, and J. D. Ward, SIAM J. Math. Anal. **38**, 574 (2006).
[76] X. Chen and E. L. Wright, Astrophys. J. **694**, 222 (2009).
[77] https://github.com/jcolinhill/pyilc/
[78] Y. Akrami *et al.* (Planck Collaboration), Astron. Astrophys. **643**, A42 (2020).
[79] F. McCarthy and J. C. Hill, Phys. Rev. D **109**, 023529 (2024).
[80] R. A. Sunyaev and Y. B. Zeldovich, Comments Astrophys. Space Phys. **4**, 173 (1972), https://ui.adsabs.harvard.edu/abs/1972CoASP...4..173S.
[81] R. A. Sunyaev and Y. B. Zeldovich, Mon. Not. R. Astron. Soc. **190**, 413 (1980).
[82] On large scales, the CMB is also correlated with unWISE galaxies due to the integrated Sachs-Wolfe (ISW) effect [83]. However, this contribution is negligible at the scales we analyze ($\ell > 300$) [84], thus we do not explicitly deproject the CMB (note that it will be still partially removed due to the NILC minimum-variance criterion).
[83] R. K. Sachs and A. M. Wolfe, Astrophys. J. **147**, 73 (1967).
[84] A. Krolewski and S. Ferraro, J. Cosmol. Astropart. Phys. 04 (2022) 033.
[85] J. Chluba, J. C. Hill, and M. H. Abitbol, Mon. Not. R. Astron. Soc. **472**, 1195 (2017).
[86] D. Lang, Astron. J. **147**, 108 (2014).
[87] A. M. Meisner, D. Lang, and D. J. Schlegel, Astron. J. **153**, 38 (2017).
[88] A. M. Meisner, D. Lang, and D. J. Schlegel, Astron. J. **154**, 161 (2017).
[89] E. F. Schlafly, A. M. Meisner, and G. M. Green, Astrophys. J. Suppl. Ser. **240**, 30 (2019).
[90] A. Krolewski, S. Ferraro, E. F. Schlafly, and M. White, J. Cosmol. Astropart. Phys. 05 (2020) 047.
[91] E. L. Wright *et al.*, Astron. J. **140**, 1868 (2010).
[92] A. Mainzer *et al.*, Astrophys. J. **731**, 53 (2011).
[93] A. S. Maniyar, M. Béthermin, and G. Lagache, Astron. Astrophys. **614**, A39 (2018).
[94] Z. Yan, A. S. Maniyar, and L. van Waerbeke, J. Cosmol. Astropart. Phys. 05 (2024) 058.
[95] https://github.com/LSSTDESC/NaMaster.
[96] E. Hivon, K. M. Gorski, C. B. Netterfield, B. P. Crill, S. Prunet, and F. Hansen, Astrophys. J. **567**, 2 (2002).
[97] D. Alonso, J. Sanchez, and A. Slosar (LSST Dark Energy Science Collaboration), Mon. Not. R. Astron. Soc. **484**, 4127 (2019).
[98] A. Nicola, C. Garcia-Garcia, D. Alonso, J. Dunkley, P. G. Ferreira, A. Slosar, and D. N. Spergel, J. Cosmol. Astropart. Phys. 03 (2021) 067.
[99] V. Anastassopoulos *et al.* (CAST Collaboration), Nat. Phys. **13**, 584 (2017).
[100] S. Hoof and L. Schulz, J. Cosmol. Astropart. Phys. 03 (2023) 054.
[101] Additional, but weaker, constraints from searches for γ-rays produced by a diffuse supernova background of axions have been obtained using *Fermi-LAT* data [102].
[102] F. Calore, P. Carenza, C. Eckner, T. Fischer, M. Giannotti, J. Jaeckel, K. Kotake, T. Kuroda, A. Mirizzi, and F. Sivo, Phys. Rev. D **105**, 063028 (2022).
[103] M. C. D. Marsh, H. R. Russell, A. C. Fabian, B. P. McNamara, P. Nulsen, and C. S. Reynolds, J. Cosmol. Astropart. Phys. 12 (2017) 036.
[104] O. Ning and B. R. Safdi, arXiv:2404.14476.
[105] C. S. Reynolds, M. C. D. Marsh, H. R. Russell, A. C. Fabian, R. Smith, F. Tombesi, and S. Veilleux, Astrophys. J. **890**, 59 (2020).
[106] J. S. Reynés, J. H. Matthews, C. S. Reynolds, H. R. Russell, R. N. Smith, and M. C. D. Marsh, Mon. Not. R. Astron. Soc. **510**, 1264 (2021).
[107] A. Arvanitaki, M. Baryakhtar, and X. Huang, Phys. Rev. D **91**, 084011 (2015).
[108] V. Cardoso, O. J. C. Dias, G. S. Hartnett, M. Middleton, P. Pani, and J. E. Santos, J. Cosmol. Astropart. Phys. 03 (2018) 043.
[109] M. Baryakhtar, M. Galanis, R. Lasenby, and O. Simon, Phys. Rev. D **103**, 095019 (2021).
[110] C. O'Hare, cajohare/axionlimits: Axionlimits, https://cajohare.github.io/AxionLimits/ (2020).
[111] S. Amodeo *et al.*, Phys. Rev. D **103**, 063514 (2021); **107**, 063514(E) (2023).
[112] E. Schaan *et al.* (Atacama Cosmology Telescope Collaboration), Phys. Rev. D **103**, 063513 (2021).
[113] A. Kusiak, B. Bolliet, S. Ferraro, J. C. Hill, and A. Krolewski, Phys. Rev. D **104**, 043518 (2021).
[114] M. S. Madhavacheril, N. Battaglia, K. M. Smith, and J. L. Sievers, Phys. Rev. D **100**, 103532 (2019).
[115] J. X. Prochaska and Y. Zheng, Mon. Not. R. Astron. Soc. **485**, 648 (2019).
[116] V. Heesen, S. P. O'Sullivan, M. Brüggen, A. Basu, R. Beck, A. Seta, E. Carretti, M. G. H. Krause, M. Haverkorn, S. Hutschenreuter, A. Bracco, M. Stein, D. J. Bomans, R.-J. Dettmar, K. T. Chyży, G. H. Heald, R. Paladino, and C. Horellou, Astron. Astrophys. **670**, L23 (2023).
[117] V. Muralidhara and K. Basu, J. Cosmol. Astropart. Phys. 11 (2024) 010.
[118] E. Osinga, R. J. van Weeren, L. Rudnick, F. Andrade-Santos, A. Bonafede, T. Clarke, K. Duncan, S. Giacintucci, and H. J. A. Röttgering, arXiv:2408.07178.
[119] R. Pakmor, R. Bieri, F. van de Voort, M. Werhahn, A. Fattahi, T. Guillet, C. Pfrommer, V. Springel, and R. Y. Talbot, Mon. Not. R. Astron. Soc. **528**, 2308 (2024).
[120] http://www.tacc.utexas.edu